OPERATION REGIMES OF FLUIDIZED BEDS

Miloslav HARTMAN[a], Zdenek BERAN[b], Karel SVOBODA[a] and Vaclav VESELY[a]

[a] *Institute of Chemical Process Fundamentals, Academy of Sciences of the Czech Republic, 165 02 Prague 6-Suchdol, The Czech Republic*
[b] *Department of Chemical Engineering, Technical University Brno, 637 00 Brno, The Czech Republic*

Received October 11, 1994
Accepted December 7, 1994

The state of the art has been reviewed in the analysis and description of flow or contacting pattern in gas–solid contacting units where a gas flows upwards through a bed of solids. The flow regime or contacting mode varies widely, depending on the particle size, particle density, gas density, gas viscosity, gas velocity and column geometry. The influence of such variables is reflected in the particle classification schemes and regime diagrams to cover the operation regions of common gas–solid re-

actors and contactors. In general, fluidized beds can be operated in six different regimes: particulate (homogeneous) fluidization, bubbling fluidization, slugging fluidization, turbulent fluidization, fast fluidization and pneumatic conveying. The bubbling beds can be further classified into three different modes of contacting: fast bubble regime, slow bubble regime and rapidly growing bubble regime. Characteristic features of all the regimes as well as the transitions between them are discussed. Current research interests, supported by practical needs, are oriented toward the operation conditions and contactor geometry of high velocity units.

1. INTRODUCTION

A fluidized bed provides a practical way of contacting particulate solids with gases or liquids. Units with fluidized beds have been in use for more than fifty years and a considerable progress has been achieved in their design and development. In the literature[1,2], commercially successful applications of fluidized bed have been described that solve the problems with the severe catalyst deactivation (e.g., the catalytic cracking method for gasoline manufacture), control of operation temperature in highly exothermic or endothermic processes (e.g., the chlorination of hydrocarbons, the roasting of sulfides and drying operations). Aside from such successful commercial applications, some technical and economic problems also occurred. Difficulties and occasional failures of fluidized bed units have usually been attributed to an unsufficient understanding of the basic physics of gas–solid fluidization. A great deal of fundamental research has been carried out that clarifies many of the pertinent features. However, systems with larger particles or those with the widely polydisperse solids and operated at high gas velocities, high temperature and/or under elevated pressure (e.g., combustion and gasification) are still relatively little understood.

Because of intensive solids mixing, temperature fields are nearly uniform within the whole volume of bed. Hot spots do not occur in the bed and the heat transfer as well the mass transfer is usually rapid. Even in the cases of strongly exothermic or endothermic processes, fluidized beds are practically isothermal with the solid particles being very well mixed. Owing to their liquid-like behavior, material of fluidized beds can easily be transferred from one vessel to another container.

The use of fluidized beds can also have some disadvantages. It requires a careful design and the prescribed conditions of operation have to be maintained. Gas mixing is not often intensive and the flow of large bubbles can considerably reduce the needed contact between the gas phase and the bed particles. There can also be the problems of particle break-up or attrition and their elutriation out of the bed. Sticky particles may agglomerate and then segregate at the bottom of the bed. Such phenomena often lead even to defluidization, i.e., to the formation of undesirable static zones of the particles at the fluidization grid.

The mode of fluidization or the regime of fluidized beds varies widely in dependence on the size and density of particles, on the physico-chemical properties and flow rate of

the employed fluid. The regimes are so different that they cannot be represented by a single hydrodynamic model. Therefore, it is useful to define and describe the basic operation modes of fluidized beds.

This article is an addition to recent studies of ours on the hydrodynamic behavior of fluidized beds[3–6].

2. GENERAL CONCEPT OF QUALITY OF FLUIDIZATION

Based on the practical experience gained from operating full-scale units for various organic processes, researchers formulated first empirical rules concerning the conditions needed for the successful operation of fluidized beds[7]. Experience suggests that spherical, finely divided, low density particles (e.g., porous catalyst particles) fluidize much better than irregular, large/dense particles. The term "good fluidization" is employed somewhat loosely and it usually means small pressure fluctuations within the bed and in the wind box (space below the bed distributor), and less tendency to form the large bubbles and slugs. Such a phenomenon of "good fluidization" is attributed to the formation of small bubbles promoted by small/light particles.

Numerous attempts have been made to establish a criterion which can predict whether a given fluid–solid system would fluidize in a particulate (homogeneous, smooth, nonbubbling) manner or in an aggregative (heterogeneous, bubbling) mode[8–10]. As a rule of thumb it may be stated that liquid fluidized systems are homogeneous in the sense that as the superficial liquid velocity is increased the particles move apart and expand in a regular homogeneous manner until they are carried out of the column. Gas fluidized systems are most often heterogeneous. In such situation, gas above the point of minimum fluidization passes through the beds in the form of gas pockets (bubbles) containing a very small fraction of particles. The general two-phase theory of fluidization assumes that the dense (emulsion) phase exhibits the same voidage as at the minimum fluidization velocity.

Although it can generally be adopted that the fluidization with liquids is more easy and smooth than that with gases, certain situations may occur when this is not the case. For example, fine catalyst particles are fluidized by gas under elevated pressure and temperature better than lead shots (ρ_s = 11 340 kg m^{-3}) fluidized with water at ambient conditions.

Recent results of more detailed studies of Foscolo et al.[9,10] confirm that the gross behavior of any fluidized system is predetermined only by two dimensionless parameters, by the Archimedes number, *Ar*, and the density ratio, ρ_s/ρ_f, (Fig. 1) or by the terminal Reynolds number, Re_t, and the Froude number, *Fr*. However, our general experience indicates that the shape of particles also has a significant influence upon their fluidization. The fluidization of spheres is more smooth than that of highly irregular and nonisometric particles.

3. GELDART'S CLASSIFICATION OF SOLID PARTICLES AND FEATURES OF THE FLUIDIZED BEDS OF THESE PARTICLES

Upon extensive experimental testing the fluidization of numerous sorts and sizes of solids, Geldart[11] proposed four more or less clearly recognizable classes of fluidization systems[11,12]. Geldart[11] divided the particles into four categories with respect to their mean size, $\overline{d}_p$, and the density difference, $\rho_s - \rho_f$, as demonstrated in Fig. 2. It should be noted that this diagram has been constructed for the behavior under ambient conditions with air as an fluidizing medium. The same labelling of the particle groups has been preserved below as in the original work of Geldart[11].

3.1. *Group C*

Group C includes very fine materials (typically with $\overline{d}_p < 20 - 30$ μm), usually cohesive powders the fluidization of which is extremely difficult. In small diameter beds, such a powder rises as a plug of solids when an attempt is made to fluidize it. It shows a strong tendency to form stable channels from the distributor to the bed surface in larger diameter columns. Such difficulties arise because the interparticle forces are greater than the forces which the fluidization medium can exert upon the particles. These considerable interparticle forces result from the very small particle size or strong electrostatic charge and are further augmented if the particle surface is sticky, wet or when the solids are soft or have a very irregular shape.

Flour, starch and talc can serve as examples of this category. Because of the above phenomena the contact between gas and solids, particle mixing and, consequently, heat

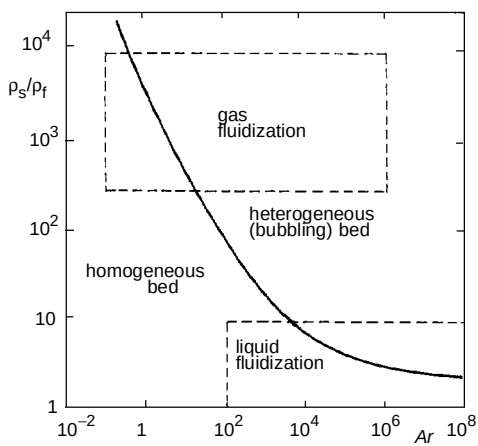

FIG. 1
Regions of homogeneous (particulate) and heterogeneous (aggregative, bubbling) beds for fluidization by any fluid[10]

transfer between a surface and the bed is quite poor. Fluidization of very fine materials can be made possible when such beds are vibrated or mechanically stirred. In such cases the plugs and stable channels are broken up and gas–solid contacting is improved[13,14].

3.2. *Group A*

Group A solids are characterized by a relatively small particle size (typically materials with $\bar{d}_p = 40 - 100$ μm) and a low particle density (typically with $\rho_s < 1\,500$ kg m^{-3}). A considerable amount of research effort was oriented to this type of powders, mainly because commercial catalytic reactors with fluidized beds employ very frequently such materials. Fluid cracking catalysts can serve as a typical example of Group A powders.

Some interparticle forces exist in Group A particles. Because of this, beds of powders in this group undergo considerable expansion at fluid velocities between the minimum fluidization velocity, U_{mf}, and the velocity at which bubbling commences (the minimum bubbling velocity, U_{mb}), i.e., $U_{mb} > U_{mf}$. As the Group A particles are slightly cohesive, a weak metastable structure of the expanded homogeneous (dense) bed can exist at $U \in \langle U_{mf}, U_{mb} \rangle$. Furthermore, the Group A powders exhibit an increase in the void fraction of the emulsion phase as the fluidizing gas velocity is increased.

Group A solids are easy to circulate in the bed and well-visible convection currents appear even when relatively few bubbles are formed within the bed. This results in rapid mixing of the whole bed. All bubbles rise more rapidly than the gas percolating through the emulsion phase, i.e., $U_b > U_e \doteq U_{mf}/\varepsilon_{mf}$. In freely bubbling beds the velocity

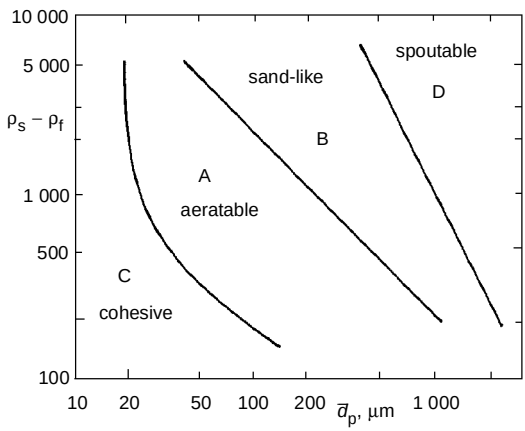

FIG. 2
The Geldart's diagram for classifying solid particles fluidized with air at ambient conditions[11]

of bubbles seems to be about 0.3 – 0.4 m s^{-1} regardless of bubble diameter. This fact suggests that the rise velocity of bubbles is controlled by the gross circulation currents.

The bubbles tend to split and coalesce very frequently which leads to a restricted bubble size. There is a maximum bubble size, usually less than 10 cm. This is a probable cause of smooth fluidization even in cases of high beds of these materials. Because of gross circulation of the bed, gas in the emulsion (dense) phase is considerably backmixed. Mass transfer between bubbles and the emulsion gas is intensive due to rapid splitting and recoalescence of the bubbles. The ratio of the cloud volume surrounding a bubble to the bubble volume is practically negligible.

3.3. *Group B*

Group B powders are most often materials with $\bar{d}_p$ = 120 – 800 μm and densities in the range 1 500 – 4 000 kg m^{-3}. In contrast to Group A particles, interparticle forces are negligible and bubbles begin to form at or only slightly above the minimum fluidization, i.e., $U_{mb} \doteq U_{mf}$. Materials of this type occur most frequently in practice. Typical examples of Group B materials are silica sand, ash and glass beads (ballotini).

Small bubbles form at the distributor and grow larger by coalescence as they move through the bed. Most bubbles rise more rapidly than the emulsion (interstitial) gas (i.e., $U_b > U_e$) and in addition to the distance above the distributor, their size increases also with the excess gas velocity, $U - U_{mf}$. In general, the ratio of the volume of cloud to the volume of bubble is not negligible and there is no experimental evidence of a maximum bubble size.

Backmixing of the emulsion (dense phase) gas as well as mass transfer between the bubbles and the emulsion phase is relatively slow. The minimum fluidization velocity of Group B particles decrease with increasing temperature[15–17].

3.4. *Group D*

Large (typically materials with $\bar{d}_p$ > 900 – 1 000 μm) and/or dense solids belong to this category of materials. The bubbles coalesce rapidly and grow to a large size. The gas velocity in the emulsion phase is high. Except for the largest ones, the bubbles move more slowly than the interstitial gas, i.e., $U_b < U_e$. Because of this, gas flows into the base of the bubble and leaves the bubble at its top. This mechanism is different from that observed with Group A and B particles.

The gas voids (bubbles) are horizontally shaped and do not bring about efficient mixing of particles. Consequently, backmixing of the emulsion gas is rather slow. The fluidization of large particles is not often stable as they tend to spout even when the bed depth is quite appreciable.

A large amount of gas is needed to fluidize Group D particles. High gas velocities can often lead to the erosion of equipment and particle attrition with rapid elutriation of

the fines produced. An important feature should be mentioned from the practical point of view. Thanks to the high particle momentum and fewer contacts among large particles, relatively sticky (wet) particles can be processed in such fluidized beds.

The minimum fluidization velocity of Groups A and B particles usually decreases with increase in temperature. In contrast to materials A and B, the minimum fluidization velocity of Group D particles is not a monotoneous function of temperature. The derivative dU_{mf}/dT can be positive as well as negative in dependence on the particle diameter and temperature[17,18]. Systems with large particles are not well-understood. Nevertheless, they are practically important as it is demonstrated by their use in the fluidized bed gasification and combustion.

3.5. *Summary*

Geldart also proposed numerical criteria to differenciate among the individual groups. However, our experience indicates that the boundaries between the groups are not sharp. Practice shows that the concept of the four broad groups of solids is useful and was widely accepted.

The majority of gas–solid reactions are carried out with Group B particles. Except for very fine, cohesive materials, the quality of fluidization deteriorates as the size and density of particles are increased. In general, increasing temperature and pressure improve appreciably the fluidized bed behavior. It is apparent that the present needs of the

TABLE I
The Geldart's classification of particles[11]

Group	Increasing size and density →			
	C	A	B	D
Typical particle size, μm	<20 – 30	40 – 100	120 – 800	>900 – 1 000
Main feature	cohesive, extremely difficult to fluidize	$U_{mb} > U_{mf}$	$U_{mb} \doteq U_{mf}$	
Example	starch	porous catalysts	silica sand	crushed limestone
Bubbles		maximum bubble size exists	no limit on bubble size	horizontal voids
Solids mixing		rapid	moderate	slow, tendency to spout
Gas mixing		rapid	moderate	slow

new advanced materials lead to considerable interest of researchers in the properties of very fine powders. In general, the range of mean particle sizes employed in commercial fluidized bed units has been broadened appreciably in the past two decades which reflects increasing interest in processing both coarse and very fine particulate materials. Basic characteristics of all four group particles is given in Table I.

Several attempts have been made to refine and modify the Geldart's classification scheme. Martin[19] and Sciazko and Bandrowski[20] extended the boundaries to different gas properties by work at elevated temperature and pressure and by using other gases than air. Efforts have also been taken by Molerus[21] and Rietema[22] to explain the differences in behavior of various types of solids and provide a basis for predicting the situations in which a given behavior can be encountered.

Distinctive fluidization characteristics represented by the Geldart diagram in Fig. 2 and by Table I reflect the complexity of gas–solid systems. In a broader context, other parameters such as the particle shape[23–25] and the size distribution of solids should also be considered in addition to the mere mean particle size $\bar{d}_p$ and densities, ρ_s and ρ_f.

4. FLOW REGIMES IN GAS–SOLID CONTACTING IN DEPENDENCE ON THE FLOW RATE OF GAS PHASE

Aside from fixed or moving packed beds, rotary drums (including rotary kilns and driers), the most popular types of equipment involve fluidized beds, and entrained flow systems. The economic and technical feasibility of different processes depends to a significant extent on understanding the physical behavior of the gas–solid reactors as well as on the physico-chemical properties of a given system.

If a fluid is blown upwards through a bed of particulate material at a superficial velocity, U, several different flow regimes are possible: packed (fixed) bed, homogeneous (particulate, bubble-free) fluidization, heterogeneous (bubbling, aggregative) fluidization, slugging, turbulent fluidization, fast fluidization (circulating bed) and dilute conveying (pneumatic transport). Some important features of comparison of the principal types of gas–solid contactors are given in Table II (ref.[26]). Physical pictures of these fluidization regimes are given in Fig. 3 in the order of increasing gas flow rate, U, and void fraction, ε.

Not every fluidized bed can go through all the fluidization regimes from the homogeneous to the fast fluidization or dilute conveying merely by increasing gas velocity. For example, the bubble free expansion occurs rarely with the gas–solid systems (see Fig. 1). Slugging is not likely to occur in larger diameter beds. Pneumatic conveying can hardly be operated with very large/heavy particles. While some of the regime transitions are sharp, easily determined by experiment and quite well correlated, others, particularly those which exist at higher superficial gas velocities, are somewhat diffusive and poorly understood.

TABLE II
Principal continuous gas–solid contactors[26]

Property	Fluidized bed	Spouted bed	Circulating bed	Entrained flow
Mean particle diameter, mm	0.03 – 3	0.8 – 6	0.05 – 0.5	0.02 – 0.08
Superficial gas velocity, m s^{-1}	0.5 – 3	0.6 – 2	3 – 12	15 – 30
Gas mixing	complex: two phases	two regions	dispersed plug flow	near plug flow
Solids mixing	usually near perfect	near perfect	rapid	near plug flow
Overall voidage	0.5 – 0.8	0.4 – 0.6	0.85 – 0.99	0.98 – 0.998
Temperature gradients	very small	may be significant	small	may be significant
Typical bed-to-surface heat transfer coefficient, W m^{-2} K^{-1}	200 – 550	150 – 250	150 – 250	50 – 100
Attrition	some	considerable	some	considerable
Agglomeration	may occur	little problem	no problem	no problem

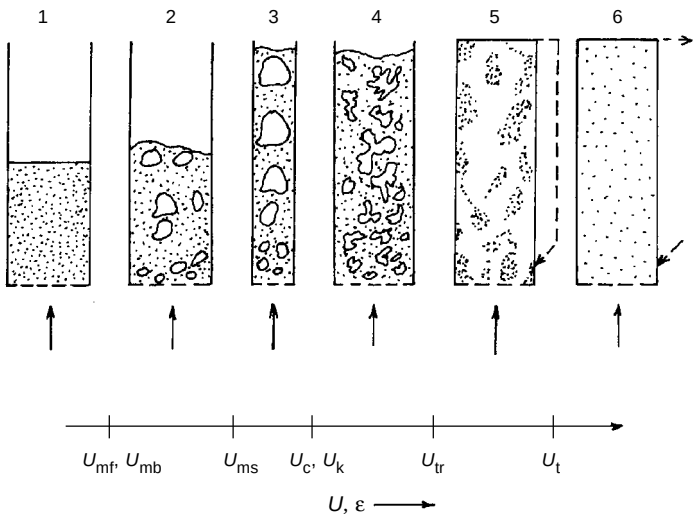

FIG. 3
Principal flow regimes for upward flow of gas through a bed of particulate solids: 1 packed bed or homogeneous fluidized bed; 2 bubbling (heterogeneous) fluidized bed; 3 slugging bed; 4 turbulent bed; 5 fast (circulating) bed; 6 pneumatic transport

4.1. *Dimensionless Groups*

For an idealized system of monosized solid particles of diameter, d_p, and density, ρ_s, fluidized at a superficial velocity, U, with a fluid of density, ρ_f, and viscosity, μ_f, the voidage of bed, ε, can be expressed as[26–30]

$$\varepsilon = f(\rho_f, \rho_s - \rho_f, \mu_f, \boldsymbol{g}, d_p, U) \quad . \tag{1}$$

Units of all the quantities employed throughout this article are given in Symbols.

In any real system, interparticle forces as well as wall effects should also be considered. It means that in practice, effects of secondary variables such as diameter and height of bed, distributor design, particle shape, particle size distribution and humidity of gas can frequently be significant. With the aid of the dimensionless groups, d_p^*, and, U^*, Eq. (*1*) is usually expressed as

$$\varepsilon = \varepsilon\,[d_p^*, U^*, (\rho_s - \rho_f)/\rho_f] \quad , \tag{2}$$

where

$$d_p^* = [\boldsymbol{g}\rho_f(\rho_s - \rho_f)/\mu_f^2]^{1/3} \tag{3}$$

and

$$U^* = U\left[\frac{\rho_f^2}{\boldsymbol{g}\mu_f(\rho_s - \rho_f)}\right]^{1/3} \quad . \tag{4}$$

It can easily be shown that the dimensionless groups, d_p^*, and, U^*, are related to the Archimedes number and the Reynolds number as follows

$$d_p^* = Ar^{1/3} \tag{5}$$

$$U^* = Re/Ar^{1/3} \quad . \tag{6}$$

The above dimensionless groups are often employed in empirical correlations of the terminal velocity and in maps of fluidization regimes (see paragraph 4.7.).

4.2. *Incipient Fluidized State*

At the onset of fluidization, the pressure drop across the bed is equal to the apparent weight of the bed particles per unit cross-sectional area of bed. An application of the Ergun capillary flow model[6] for the pressure drop across a fixed bed of isometric particles leads to the final dimensionless relationship

$$\frac{1.75}{\varepsilon_{mf}^3 \psi} Re_{mf}^2 + \frac{150(1-\varepsilon_{mf})}{\varepsilon_{mf}^3 \psi^2} Re_{mf} - Ar = 0 \quad . \tag{7}$$

In its essence, the Ergun equation (*7*) is a reasonable extrapolation of the fixed (static) bed state to the minimum fluidization conditions represented by Re_{mf}. The bed voidage at the onset of fluidization, ε_{mf}, is slightly larger than that in a fixed bed. It can be estimated from random packing data or can be determined by experiment. It should be noted that the predictions of the minimum fluidization velocity provided by the Ergun equation are very sensitive to the minimum fluidization bed voidage, ε_{mf} (ref.[6]).

The onset of fluidization was a subject of numerous investigations in the past years. We have treated in detail this state of fluidized bed in our recent comprehensive study[6]. In most cases, the minimum fluidization velocity can be predicted with the use of empirical correlations[12,31] in the form

$$Re_{mf} = (C_1^2 + C_2 Ar)^{0.5} - C_1 \tag{8}$$

with an average accuracy of ±25%. As Eq. (*7*) suggests, the parameters C_1 and C_2 are functions of the bed voidage, ε_{mf}, and the particle sphericity, ψ. Values of the parameters C_1 and C_2 are tabulated for various materials in ref.[6]. The less spherical or less isometric the particles are, the lower accuracy is exhibited by empirical expressions such as Eq. (*8*). Relationships (*7*) and (*8*) are based upon the experimental work at ambient conditions. Nevertheless, they also provide satisfactory results for elevated pressure and temperature when the influence of these variables on the fluid density and viscosity is accounted for[6].

It should be emphasized that the above concept of the minimum fluidization velocity loses its sens in the case of widely multicomponent or polydisperse fluidized beds. Instead of U_{mf}, the complete fluidization velocity, U_{cf}, is employed that is defined as the velocity at which all the particles are fully engaged or supported by the gas. It is

apparent that all the predictive equations necessarily fail when phenomena such as agglomeration or sticking of particles occur.

4.3. *Homogeneous (Particulate) Fluidization*

When very fine particles belonging to Geldart's Group A particles are fluidized with gas, the bed can expand to a certain extent without forming voids (bubbles). The bed expands homogeneously (smoothly) until a velocity is reached at which first small bubbles appear at the bed surface. The average of the superficial velocities at which the bubbles appear (when U is gradually increased) and disappear (when U is gradually reduced) is called the minimum bubbling velocity, U_{mb}.

The homogeneous expansion can occur only in beds of light and small particles (0.030 – 0.100 mm). As the particle size increases, the region of the homogeneous fluidization is narrowed. With a certain particle size, the region of the smooth expansion vanishes in the so-called tripple point[32]. Such a situation is depicted in Fig. 4. The Archimedes number corresponding to the tripple point amounts to about $Ar = 100$. Such a value suggests an approximate upper limit of possible occurrence of the bubble-free expansion in the gas–solid fluidized systems. Experimental results indicate that the range of homogeneous, bubble-free expansion at gas velocities between U_{mf} and U_{mb} increases significantly with increasing pressure[33,34].

In their attempts to correlate the porosity of homogeneous bed fluidized with gas, Davies and Richardson[35] employed the approach originally developed by Richardson and Zaki[36] for liquid–solid fluidization[37–40]

$$Re / Re_t = \varepsilon^n \quad . \tag{9}$$

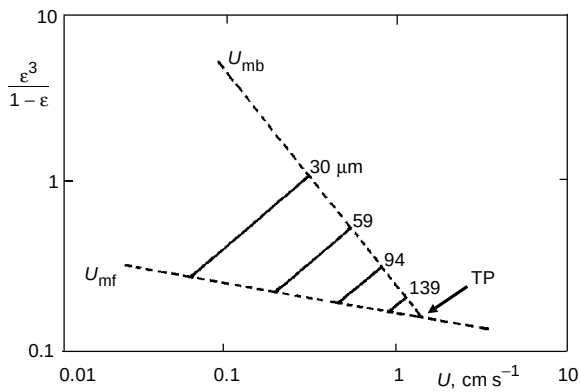

FIG. 4
Region of the homogeneous gas fluidization (smooth expansion) for the catalyst particles of different size: ρ_s = 800 – 900 kg m^{-3} (ref.[32]), TP tripple point

The exponent n is a complex function of the terminal velocity Reynolds number, Re_t, and also of the particle-to-bed ratio, d_p/D, if wall effects are significant. The terminal velocity Reynolds number, Re_t, reflects the steady state, the free-fall conditions of an isolated particle moving in an infinite fluid. It can be estimated with the aid of various relationships which we have recently reviewed[5]. Considerable progress has also been made in the case of nonspherical, isometric particles[24,25,41].

The form of Eq. (*9*) can also be employed for gas–solid systems. However, in difference to the liquid fluidization, where $n \in \langle 2.3;5.2\rangle$ (ref.[38]), higher experimental values of $n \in \langle 3.8;19.7\rangle$ have been reported for the gas fluidization where $Re \in \langle Re_{mf}, Re_{mb}\rangle$ (ref.[42]).

A different approach to the correlation of the porosity of homogeneous bed fluidized with gas, ε, that employs the Kozeny–Carman relationship was used by Abrahamsen and Geldart[43]

$$\frac{\varepsilon^3}{1-\varepsilon}\frac{(\rho_s-\rho_f)\boldsymbol{g}d_p^2}{\mu_f} = 210(U-U_{mf}) + \frac{\varepsilon_{mf}^3}{1-\varepsilon_{mf}}\frac{(\rho_s-\rho_f)\boldsymbol{g}d_p^2}{\mu_f} \quad \text{for} \quad U \in \langle U_{mf}, U_{mb}\rangle \ . \tag{10}$$

As mentioned above, the mode of particulate fluidization occurs rarely with the gas–solid systems in which the density ratio, ρ_s/ρ_f, is high. If the density ratio is low, as with the most liquid–solid systems, then the system usually behaves in the particulate mode. The phenomenon of the possible transition from particulate to bubbling liquid fluidization was firstly explored by Wallis[8]. Brandani and Foscolo[10] analyzed the stability of a particle bed model and under some simplifying assumptions, they developed the following stability criterion for a homogeneously expanded liquid–solid bed:

$$\left(\frac{Ar}{\rho_s/\rho_f}\right)^{1/2} - \left(\frac{1-\varepsilon}{3.2}\right)^{1/2} n\varepsilon^{n-1}Re_t \begin{cases} > 0; \text{ stable} \\ = 0; \text{ stability limit} \\ < 0; \text{ unstable} \end{cases} . \tag{11}$$

Practice suggests that the relationship (*11*), illustrated in Fig. 1, should be viewed as an approximative rule rather than a truly predictive expression.

4.4. *Bubbling Bed*

The formation, properties and movement of bubbles (heterogenities, gas pockets, voids) are dominant factors that determine the overall behavior of a fluidized bed. Although they have been a subject to numerous investigation the reasons for their origin and subsequent behavior in the fluidized bed are still unclear.

In describing the bubbling fluidized beds, it is essential to distinguish between the bubble phase (lean phase, bubbles containing practically no solids), and the emulsion phase (dense or particulate phase) consisting of virtually all bed particles that are fluidized by interstitial gas. It is a characteristic feature of the bubbling bed regime that the emulsion phase forms a continuous medium between discrete gas pockets. However, it is not the case of the flow regimes observed at high gas velocities.

The simple two-phase theory assumes that all gas in excess of that required for incipient fluidization passes through the bed as a visible bubble flow. Experimental observations indicate that the visible bubble flow is somewhat less than the simple two-phase theory assumes and tends to increase with the distance above the distributor. It appears that the division of gas flow between the two phases of a fluidized bed and a question which factors determine this division are still open to further studies.

The ascending bubbles bring about motion of the emulsion phase which is the main cause of solids mixing in bubbling fluidized beds. Such intensive particle motion results in the temperature uniformity and rapid bed/surface heat transfer. It is also apparent that the mass transfer between discrete bubbles and emulsion gas in the continuous phase can strongly effect the performance of a fluidized bed unit. In some situations, bubbles can be the cause of serious gas bypassing of the solids which can result in a low chemical conversion of reactants. Although some similarities exist, gas pockets in fluidized beds are in many ways different from gas bubbles in liquids.

The problems of bubbles in gas–solid beds are extensive and for their general treatment the reader is rather referred, for example, to the monographs of Yates[1] and Kunii and Levenspiel[2].

Experience gained with larger fluidized beds suggests that three different zones can be distinguished within a bubbling bed: a distributor zone with the horizontal/vertical jets of gas or with very small bubbles, bubbled bed and a surface zone in which the bubbles burst throwing some particles into the freeboard.

The lowest gas velocity at which bubbles are still formed is denoted as the minimum bubbling velocity or the minimum bubbling point, U_{mb}. It is typical of Geldart's Group B and D particles that bubbling starts very close to the point of minimum fluidization, i.e., $U_{mb} \doteq U_{mf}$. Unlike the Group B and D materials, Group A powders exhibit an increase in the porosity of the emulsion phase as the gas velocity increases. Consequently, the minimum bubbling velocity is always greater than the minimum fluidization velocity, i.e., $U_{mb} > U_{mf}$.

By regression analysis of a large amount of their experimental data on U_{mb} Broadhurst and Becker[44] proposed a correlation

$$\frac{\gamma d_p}{\rho_f U_{mb}^2} = 98\,000 \left(\frac{\mu_f^2}{\rho_f \gamma d_p^3} \right)^{0.82} \left(\frac{\rho_s}{\rho_f} \right)^{0.22} + 35.4 \qquad (12)$$

for $500 < \rho_s/\rho_f < 50\,000$ and $1 < \rho_f \gamma d_p^3/\mu_f^2 < 10^7$. Equation (*12*) correlates the minimum bubbling velocity with an accuracy of ±25%. In terms of Re_{mb} and Ar, Eq. (*12*) can be rewritten as follows

$$Re_{mb} = \left[\frac{Ar^{1.82}}{35.4\, Ar^{0.82} + 98\,000\, (\rho_s/\rho_f)^{0.22}} \right]^{1/2} . \qquad (13)$$

The authors[44] described the variation in the void fraction at the minimum bubbling point by

$$\varepsilon_{mb} = \frac{0.586}{\psi^{0.72}\, Ar^{0.029}}\, (\rho_f/\rho_s)^{0.021} \qquad (14)$$

for $0.85 < \psi < 1$, $1 < Ar < 10^5$ and $500 < \rho_s/\rho_f < 50\,000$. As can be seen, the particle sphericity is the major factor determining ε_{mb}.

As a general rule, ε_{mb} is predicted from Eq. (*14*) with a probable error of about ±0.02, provided that the estimated value is greater than about 0.4. Smaller values may be physically unrealistic.

The bubbling bed expansion[45,46] is closely related to the bubbling phenomena in such fluidized beds. It means that physical considerations on the bed expansion include aspects such as bubble formation at a given distributor, bubble coalescence and splitting, bubble frequency, bubble growth, possible slugging, size distribution of bubbles, rise velocity of bubbles, division of the ascending gas between the bubble and emulsion phase. In general, these phenomena are or can be dependent upon a number of different factors such as average size, density and shape of particles, particle size distribution, gas density and viscosity, bed geometry, presence of internals in the bed, operating temperature and pressure, interparticle forces and electrostatic effects. All the above circumstances contribute, particularly in their combination, to the complexities of the bubbling phenomena, which are still far from being fully understood.

In the beds of particles belonging to Groups B and D of Geldart's classification, bubbles are formed immediately beyond the point of minimum fluidization. As a general rule, it is assumed that the porosity of the dense phase does not change with gas velocity and remains equal to the bed voidage at the point of minimum fluidization, ε_{mf}. For such a bed we can express the rising velocity of bubbles at a given distance above the distributor, h, as

$$U_b = y\, (U - U_{mf})/\varepsilon_b . \qquad (15)$$

The experimental experience suggests that y is often smaller than unity and can vary with the distance above the distributor, i.e., $y = y(h)$. The simple two-phase models assume, however, that all gas in excess of that required for incipient fluidization passes through the bed as a visible bubble flow, i.e., $y = 1$.

A schematic drawing in Fig. 5 shows the bubbling fluidized bed with a perforated gas distributor.

On substituting

$$\bar{\varepsilon}_b = (H - H_{mf})/H \tag{16}$$

we can write for the height of expanded bed

$$H = H_{mf} + (U - U_{mf}) \int_0^H \frac{y}{U_b} \, dh \ . \tag{17}$$

On the basis of experimental observations, Hilligardt and Werther[47] have modified the frequently employed relationship of Davidson and Harrison[48] for the bubble rise velocity as follows

$$U_b = y\,(U - U_{mf}) + 0.711\delta(\boldsymbol{g} d_b)^{1/2} \ , \tag{18}$$

where

$$d_b = d_{b0}\,[1 + 27\,(U - U_{mf})]^{1/3}\,(1 + 6.84h)^{1.2} \ . \tag{19}$$

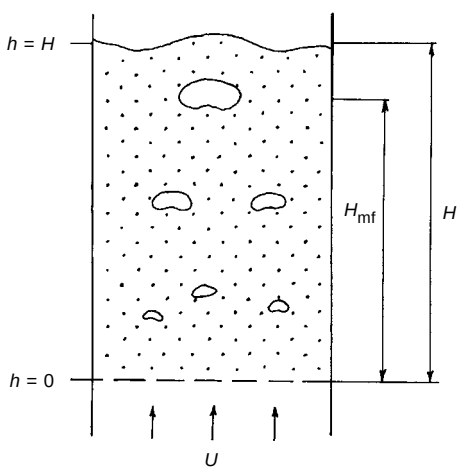

FIG. 5
Schematic drawing of an expanded bubbling bed

Although the validity of the original equation of Davidson and Harrison[48] is questioned it is widely used in fluidized bed modelling and design.

While the parameter y expresses the deviation of the visible bubble flow from the simple two-phase theory, the empirical parameter of Hilligardt and Werther[47], δ, accounts for the formation of bubble paths that are typical of fluidized bed with larger diameters (e.g., "gulf-streaming"). In general, both parameters depend on the bed dimensions and physical properties of the solids. For the sand particles from Geldart's Group B ($\overline{d}_p$ = 0.48 mm, ρ_s = 2 640 kg m^{-3}, U_{mf} = 0.18 m s^{-1}) fluidized with air at ambient conditions, the authors[47] described the hydrodynamic parameters d_{b0}, y and δ as follows

$$d_{b0} = 0.0123\ \mathrm{m}$$

$$y = 0.26 \qquad \text{for} \quad h/D < 0.55$$

$$y = 0.35\,(h/D)^{0.5} \quad \text{for} \quad 0.55 \le h/D \le 8$$

$$\delta = 0.87 \qquad \text{for} \quad 0.1\ \mathrm{m} \le D \le 1\ \mathrm{m}\ . \qquad (20)$$

It should be mentioned that in addition to Eq. (*19*) there are a number of other, also entirely empirical, correlations for estimating the bubble diameter, d_b. Such expressions usually correlate the bubble diameter as a function of the excess gas velocity, $(U - U_{mf})$, and the distance above the gas distributor, h:

$$d_b \approx (U - U_{mf})^{0.4-0.5} \qquad (21)$$

$$d_b \approx h^{0.7-0.8}\ . \qquad (22)$$

Comparison of some, often used correlations[47,49–51] for the bubble size was made in a work of ours[45]. As should be expected, the rate mass transfer between bubbles and emulsion gas is very strongly effected by the bubble diameter.

Equation (*17*) implicitly defines the height of an expanded bed, H, and can usually be solved numerically for H without any difficulty in combination with Eqs (*18*) – (*20*) or together with any other expressions for U_b and d_b. Predictions of Eqs (*18*) – (*20*) are confronted with the experimental results of Hillegardt and Werther[47] in Fig. 6.

The average height of a fluidized bed is difficult to determine, because the bed surface is subject to large fluctuations of variable amplitudes and frequencies. Several purely empirical correlations were also proposed for predicting the bed expansion.

Tamarin and Teplickii[52] have fitted the experimental data amassed with different solids and columns by the following, very simple expression:

$$H/H_{mf} = 1 + 0.327\, H_{mf}\, (U - U_{mf})^{0.667}/D^{0.5} \qquad (23)$$

for $0.5 < H_{mf}/D < 2$.

Babu et al.[53] also presented a simple equation, which incorporates the effect of some physical properties of the system

$$\frac{H}{H_{mf}} = 1 + 14.3\, \frac{d_p^{1.01} \rho_s^{0.376} (U - U_{mf})^{0.737}}{U_{mf}^{0.937} \rho_g^{0.126}} \quad . \qquad (24)$$

While the real effect of some quantities present in Eqs (*23*) and (*24*) may be questioned, it is of interest to note that the exponent at the excess gas velocity, $(U - U_{mf})$, is close to a value of 0.7 in both correlations (*23*) and (*24*).

As can be seen from Fig. 6, there are appreciable differences in predictions of the bed expansion provided by different relationships. The experimental data points plotted in Fig. 6 were measured on sharp edged and irregular in shape particles of ceramsite and with the experimental column of a smaller size (D = 0.14 m) (ref.[46]).

In dependence on the particle size and gas velocity, the bubbling bed can occur in three different regimes: fast bubbles, slow bubbles and rapidly growing bubbles[54].

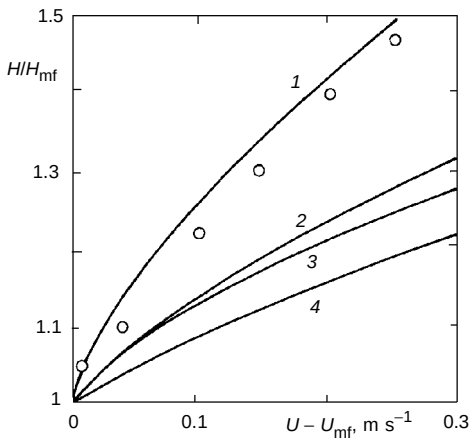

FIG. 6
Comparison of the bed expansion measured on the ceramsite particles–air system with the predictions of different relationships. Experimental data points (○), D = 0.14 m, H_{mf} = 0.13 m, $\bar{d}_p$ = 1 mm, ref.[46]. The solid lines show the bed expansion ratio computed from different expressions. *1* Hartman et al.[46]; *2* Babu et al.[53]; *3* Tamarin and Teplickii[52]; *4* Hilligardt and Werther[47]

4.4.1. Regime of Fast Bubbles

A fast bubble exists in a fluidized bed when the gas percolating through the emulsion phase moves upward more slowly than the bubble, i.e.,

$$U_e \doteq U_{mf}/\varepsilon_{mf} < U_b \ . \qquad (25)$$

Gas enters the lower part of the bubble and leaves at the top. Then, it is swept around and returns forming a cloud around the bubble. The existence of fast bubbles is characteristic for beds of fine and moderately fine particles (usually less than about 0.5 mm in diameter). Majority of the two-phase models were developed for the regime of fast bubbles. These models assume that most of the gas which passes through a bubble recirculates back to the bubble. The recirculated gas facilitates the mass transfer and the size of the cloud surrounding a bubble effects the rate of gas exchange between the bubbles and the emulsion phase. Fast bubbles have appreciable wakes of solids trailing behind them.

4.4.2. Regime of Slow Bubbles

In beds of coarse particles, the fluidizing gas percolates through the emulsion phase with a velocity an order of magnitude greater than in the beds of fine particles. Because of this, the nature of fluidization is different. Gas may rise through the emulsion at a velocity larger than the rise velocity of the bubbles, i.e.

$$U_e > U_b \ . \qquad (26)$$

Slow bubbles can occur in a bed of large particles (fluidized bed combustors and gasifiers) the minimum fluidization velocity of which is high. The recirculating gas is absent and the interstitial gas employs the bubbles as a shortcut on its way through the bed. There is evidence that the slow bubbles have considerably smaller wakes of solids than do the fast bubbles. Unlike the fast bubbles, the slow bubbles tend to coalesce rather horizontally than vertically. Such horizontal voids move rather slowly. Consequently, the rate of solids mixing as well as the extent of gas backmixing is far lower than in the fluidized beds of fine particles. It is very likely that the gas convective component will be a more important factor than heat transfer due to the motion of particles in large particle beds. Gas stream-lines in a fast and a slow bubble are shown in Fig. 7.

4.4.3. Regime of Fast Growing Bubbles

The regime of rapidly growing bubbles is attained at higher gas velocities when the rate of bubble growth is of the same magnitude as the bubble rise velocity:

$$\mathrm{d}(d_\mathrm{b})/\mathrm{d}\tau \geq U_\mathrm{b} \quad . \tag{27}$$

Large pressure fluctuations occur in this regime with amplitudes similar to the average pressure drop accross the bed. This regime was observed in shallow beds of large particles ($H < D$). In deeper beds, particularly in smaller vessels, bubbles can span the entire cross section of the column and slugging occurs.

The regime of fast growing bubbles exhibits a high overall voidage which means that an accumulation of mass in the bubbles cannot generally be neglected in the conservation equations.

4.4.4. Mapping of the Bubbling Regimes

The velocity of gas in the emulsion phase can be estimated from Eq. (*25*) where $\varepsilon_\mathrm{mf} \doteq 0.4$. The only available correlation for the diameter of bubbles in large particle beds is that of Cranfield and Geldart[55]:

$$d_\mathrm{b} = 2.25\,(U - U_\mathrm{mf})^{1.11} h^{0.81} \quad . \tag{28}$$

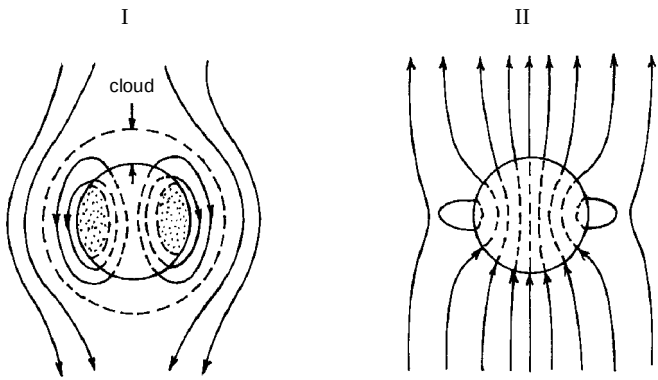

FIG. 7
Gas streamlines in a fast bubble (I) and a slow bubble (II)

It differs appreciably from the above bubble growth expression developed for fine particle beds. Comparison of Eq. (*28*) with the expression (*21*) indicates that the bubble diameter increases with the excess gas velocity much faster in large particle beds than in small particle beds.

Using the approach of Catipovic et al.[54], the criterion for slow to fast bubbles transition, which satisfies Eqs (*25*) and (*27*), can take the form

$$U - U_{\mathrm{mf}} = 0.593\, U_{\mathrm{mf}}^{1.802}/h^{0.730} \ . \qquad (29)$$

In a situation when the bubble diameter grows as rapidly as the bubble rises, it holds

$$\frac{\mathrm{d}(d_{\mathrm{b}})}{\mathrm{d}h}\frac{\mathrm{d}h}{\mathrm{d}\tau} = U_{\mathrm{b}} \ . \qquad (30)$$

As $\mathrm{d}h/\mathrm{d}\tau = U_{\mathrm{b}}$, Eq. (*30*) is equivalent to

$$\mathrm{d}(d_{\mathrm{b}})/\mathrm{d}h = 1 \ . \qquad (31)$$

With the use of Eq. (*28*) we get after some arrangement the condition for the appearance of fast growing bubbles:

$$U - U_{\mathrm{mf}} = 0.581\, h^{0.171} \ . \qquad (32)$$

With the aid of the correlation of Broadhurst and Becker[44] for the onset of fluidization

$$Re_{\mathrm{mf}} = \left[\frac{Ar^{1.85}}{37.7Ar^{0.85} + 2.42\,.\,10^5(\rho_s/\rho_{\mathrm{f}})^{0.13}}\right]^{1/2} \qquad (33)$$

boundaries of the respective regimes were estimated. The results are plotted in Fig. 8 in terms of the excess gas velocity, $(U - U_{\mathrm{mf}})$, bed height, h, and particle diameter, d_{p}. As can be seen, there exists for each bed height a certain particle diameter above which the regime of slow bubbles changes directly to the regime of fast growing bubbles.

As the particle density decreases, the boundary lines between slow and fast bubbles move downward. It should be realized that Fig. 8 can serve as a useful means of distinguishing between the respective regimes whose boundaries are not usually sharp. The

diagram is valid provided that slugging does not occur, i.e., the particles are fluidized in a large diameter bed.

Practically all existing models of the fluidized beds were developed for the fast bubble regimes, i.e., for the beds of fine particles. However, coarse particles are likely to be in the slow bubble or the in fast growing bubble regime. Different hydrodynamic behavior has to be considered when fluidized beds of coarse particles are explored and modeled.

4.5. *Slugging Bed*

In deeper fluidized beds of smaller diameter, the process of bubble coalescence can result in the formation of bubbles the size of which is close or even equal to the bed diameter. Such a situation corresponds to the onset of slugging and the formed voids are called slugs. In contrast to normal bubbles, the slugs rise more slowly than bubbles of similar size. It should be emphasized that the occurrence of slugs is accompanied by considerable deterioration in both the intensity of bed mixing and the quality of gas–solids contacting. Moreover, the motion of slugs causes large pressure fluctuations that may be mechanically damaging to equipment. The point of minimum slugging is vizualized in Fig. 9.

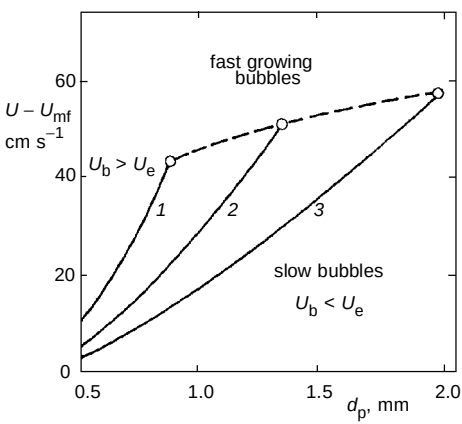

FIG. 8
Bubble regimes of coarse particle beds fluidized in a large diameter column. The curves satisfy Eqs (*29*), (*31*), (*32*) and (*33*) for ρ_s = 2 600 kg m^{-3} (sand) and ρ_f = 1.2 kg m^{-3} (air). The broken line represents the boundary of the rapidly growing bubble regime for different bed heights and particle size. Bed height (h in cm): *1* 20, *2* 50, *3* 100

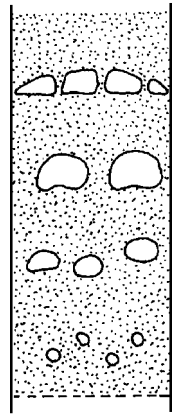

FIG. 9
The onset of slugging

Experience indicates that the slugging is easily observed and measured in beds with the aspect ratio, $(H_s/D) > 2$. The slugging does not occur at $(H_s/D) < 1$ except for beds with very large or heavy particles. In beds of Geldart's Group A fine and light particles, axisymmetric slugs are formed with the round heading edge. Particles move down in the space between the slug and the column wall. In the case of coarse, high density particles, flat-nosed slugs are formed through which the particles fall down. At high gas velocities, the flat-nosed slugs may be transformed into the asymmetric wall slugs.

The onset of slugging is usually determined by visual observations. Broadhurst and Becker[44] defined the onset of slugging as a situation reached when bubbles, before they arrive at the top of the bed, are seen to have a continuous floor around the circumference of the vessel. The onset of slugging can also be established by spectral analysis of pressure fluctuations within the bed. Such an instrumental means is based on the simple fact that higher frequences in the power spectrum are strongly diminished at the point of minimum slugging[56].

Bayens and Geldart[57] observed that the formation of slugs is markedly effected by the bed height in situations when it does not reach the critical value H_L. The authors correlated the critical bed height by

$$H_L = 1.343\, D^{0.175} \tag{34}$$

and proposed Eq. (*35*):

$$U_{ms} = U_{mf} + 0.07\,(\boldsymbol{g}D)^{1/2} + 0.163\,(H_L - H_s)^2 \ . \tag{35}$$

An extensive investigation of slugging was made by Broadhurst and Becker[44]. The authors conducted the experiments in columns 2.5 – 25 cm in diameter. Bed heights ranged from 1 to 60 column diameters, and particle diameters from 0.07 to 1.1 mm. Broadhurst and Becker[44] correlated their experimental data with the aid of the dimensionless equation

$$\frac{\rho_f U_{ms}^2}{\gamma d_p} = 51.4\left(\frac{D}{H_s}\right)^{1.79}\cdot\left(\frac{\rho_f}{\rho_s}\right)^{1.09} + 0.00416\left(\frac{\rho_f \gamma d_p^3}{\mu_f^2}\right)^{0.41}\cdot\left(\frac{\rho_f}{\rho_s}\right)^{0.59} \tag{36}$$

for $1 < H_s/D < 40$, $500 < \rho_s/\rho_f < 15\,000$, and $1 < d_p^3\,\gamma\,\rho_f/\mu_f^2 < 40\,000$. Equation (*36*) estimates the onset of minimum slugging with an accuracy of ±25%. It can easily be rewritten in terms of Re_{ms} and Ar:

$$Re_{ms}^2 = Ar\left(\frac{\rho_f}{\rho_s}\right)^{0.59}\left[51.4\left(\frac{D}{H_s}\right)^{1.79}\cdot\left(\frac{\rho_f}{\rho_s}\right)^{0.50} + 0.00416\,Ar^{0.41}\right] . \tag{37}$$

Equations (*36*) and (*37*) indicate that the superficial gas velocity at the point of minimum slugging, U_{ms}, depends strongly on the ratio of bed height and vessel diameter (aspect ratio). The ratio of the gas and solids densities also exerts a significant effect.

With the aid of Eqs (*33*) and (*37*), the onsets of fluidization, U_{mf}, and slugging, U_{ms}, were predicted in dependence on the particle diameter for $(H_s/D) = 1$. The results plotted in Fig. 10 show that even at such a shallow bed the operation region of the bubbling bed, bounded by U_{mf} and U_{ms}, is not wide. Moreover, the difference $(U_{ms} - U_{mf})$ further narrows with increasing particle diameter. Experience indicates that the difference $(U_{ms} - U_{mf})$ is somewhat enlarged at elevated temperatures.

Slugging is usually an undesirable phenomenon which is very likely to occur in many laboratory-scale reactors. In interpreting such results, the fundamental hydrodynamic differences must be taken into account between slugging and freely bubbling beds.

4.6. *Turbulent Fluidization*

The concept of fluidized bed has traditionally been linked with the regime of freely bubbling fluidization occurring at relatively low gas velocities. In this mode of operation, the two-phase structure of bed is well-developed and the contact between the phases may not be as effective as desirable. Low gas flow rates lead to an equipment of large cross-sectional area and the bed mixing can be insufficient.

Using a capacitance probe Lanneau[58] found that the two-phase character of fluidized bed diminishes and the interphase contact is improved at high gas velocities. Experience indicates a considerable interest in fluidized beds operated at high gas velocities in hydrodynamic regimes beyond the slugging regimes (e.g., ore roasting and acrylonitrile manufacture with catalytic fluid bed reactors).

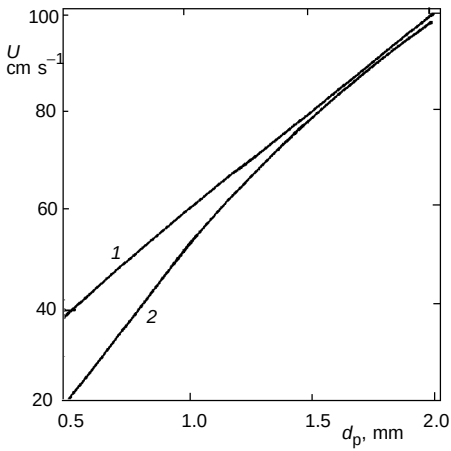

FIG. 10
Superficial gas velocity at the onset of fluidization and slugging in dependence on the particle diameter. Curves show the predictions of Eqs (*33*) and (*37*) for $\rho_s = 2\ 600$ kg m^{-3}, $\rho_f = 1.2$ kg m^{-3} and $H_s/D = 1$. *1* U_{ms}, *2* U_{mf}

Kehoe and Davidson[59] observed a breakdown of slugging in a bed of fine particles as the gas velocity was increased. At a certain gas flow rate the slugging bed passed to a state characterized by the occurrence of zig-zag moving tongues of gas. Discrete bubbles or gas pockets does not appear in the bed. Turbulent fluidization has also been seen as a transition between lower velocity mode (bubbling or slugging) where voids are dispersed in the dense emulsion phase and a high velocity regime (fast fluidization) where dense clusters or strands are dispersed in a dilute phase[60,61].

The surface of turbulent bed is much more diffusive than that of freely bubbling bed because of considerable entrainment of particles. The turbulent bed remains relatively dense with the porosity about 0.7.

Indicators which have been employed to identify the onset of the turbulent fluidization include visual appearance, local capacitance, bed expansion and pressure fluctuations. Measurements of pressure fluctuations have been used most frequently[61]. As the gas velocity is increased, the amplitude of pressure fluctuations as well as the void fraction increases in the slugging or bubbling bed. At a certain superficial gas velocity, which is often called U_c (ref.[62]), the amplitude of pressure fluctuations reaches a maximum. Below U_c, the two-phase structure of fluidized beds is clear and the gas voids grow larger with increasing gas flow rate. The quantity U_c is marked by the beginning of the breakdown of bubbling and decrease of the amplitude of pressure fluctuations. Above U_c, the fluidized bed gradually gives way to a condition of increasing uniformity that culminates in a turbulent state. Complete transition to the turbulent regime occurs at a superficial velocity U_k, where large discrete voids are absent and the amplitude of pressure fluctuations has levelled off[62,63].

Researchers are not in general agreement on the real point of transition to the turbulent fluidization regime. It appears that the mode of this transition is determined best by the both characteristic velocities U_c and U_k.

Yerushalmi and Cankurt[62] measured the regime transitions with the particles between 0.030 and 0.270 mm.

The two superficial velocities U_c and U_k increase with increasing particle size and particle density. The experimental values of U_c and U_k approximately follow a linear dependence on the term $(\rho_s\, d_p)^{1/2}$. These dependences are shown and compared to the similar results of Staub and Canada[64] in Fig. 11. As can be seen the findings of Staub and Canada[64] are between the bounds represented by U_c and U_k. Bi and Fan[63] proposed a correlation for the onset of the turbulent regime expressed by

$$Re_k = 0.601\, Ar^{0.695}\ ,\ \text{for}\ \ Ar \le 125 \qquad (38)$$

and

$$Re_k = 2.28\, Ar^{0.419} \ , \ \text{for} \ \ Ar \geq 125 \ . \qquad (39)$$

It should also be noted that the transition from bubbling to turbulent fluidization significantly moves to lower gas flow rates with increasing column diameter. Moreover, this transition is achieved more early for the wide distribution solids than for narrow fractions of particles[64].

The structure of a turbulent fluidized bed of fine particles is formed by two interacting phases. Neither phase can be considered as continuous or discrete. The dense phase includes closely arranged clusters of the particles, the lean phase contains single particles as well as their small aggregates. The existence of clusters is the apparent cause of the fact that the velocities U_c and U_k are greater that the terminal velocity of isolate particles U_t.

In Table III the ratios U_c / U_t are given for various materials. As can be seen the values of U_c for very small particles are by an order of magnitude greater than the terminal, free-fall velocity of the isolated particles. The ratio U_c / U_t decreases as the particle diameter is increased. It is less than unity when the clusters of particles are not formed.

4.7. *Fast Fluidization (Circulating Bed)*

While the lower bound of the turbulent regime is represented by the characteristic velocities U_c and/or U_k, the upper limit is defined by the transport velocity U_{tr}. As the gas flow rate is approaching this velocity, the rate of entrainment from the top of the vessel markedly increases so that it becomes essential to capture and return the entrained solids (circulating beds) or to feed fresh solids to the bottom of the column (pneumatic

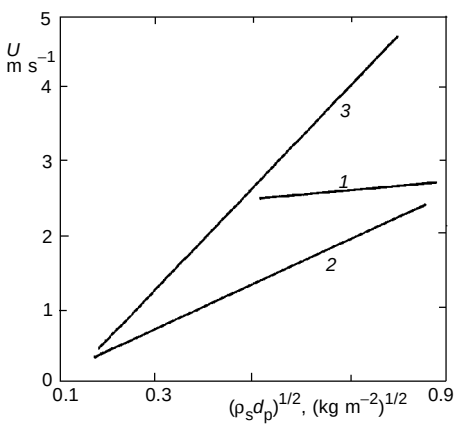

FIG. 11
Transition to turbulent fluidization bounded by the characteristic gas superficial velocities U_c (*2*) and U_k (*3*) (ref.[62]). Line *1* shows the results of Staub and Canada[64]

transport). Such a situation occurs when the gas superficial velocity is greater than the terminal velocity of a considerable fraction of the particle clusters. The transport velocity in the systems with small particles is often by an order of magnitude greater than the terminal velocity corresponding to the mean size of particles. In the systems with larger particles, the transport velocity is close to the terminal velocity of an average single particle.

The regime of fast fluidization is most often considered as a mode of fluidization where there is no longer a distinct interphase between a dense bed and a diluted freeboard region. Instead, there is a gradual increase in void fraction over the height of the column. It is practical to distinguish between the regime of fast fluidization and the flow characteristics encountered in riser or transport bed reactors. While the fast fluidized bed contains typically 2 to 15% by volume solids, the flow in transport bed reactor is more dilute usually with 1 to 5% by volume solids[64]. There is no general approach capable of predicting the transition to the fast fluidization regime. Similarly as with the transition to turbulent fluidization, the transition to fast fluidization is gradual rather than sharp. A typical regime of fast fluidization is characterized by a gas velocity that is moderately greater than the transport velocity, U_{tr}, and by a rapid recirculation of solids.

The regime of fast fluidization is characterized by a high degree of particle turbulence. As a measure of gas–solid interacting can serve the slip velocity, U_{sl}, defined as

$$U_{sl} = U/\varepsilon - U_s \qquad (40)$$

TABLE III
Onset of transition to the turbulent fluidized bed[64–66]

Material	d_p, μm	ρ_s, kg m^{-3}	ψ	U_t, m s^{-1}	U_c, m s^{-1}	U_c/U_t
Dicalit 4200	33	1 670	0.4	0.0227	0.53	23.4
Catalyst	49	1 070	1.0	0.0778	0.61	7.84
Catalyst	49	1 450	1.0	0.106	0.91	8.58
Alumina	103	2 460	1.0	0.582	1.22	2.10
Sand	268	2 650	0.82	1.16	2.74	2.36
Ballotini	>100 <650				2.5 – 3.0	0.55 – 0.65
Ballotini	1 000	2 770	1.0		4.0	0.459

rather than the superficial gas velocity *U*. Aside from the gas flow rate, the volume concentration of particles is also strongly effected by the rate of their feeding to the column.

The experimental data of Yerushalmi and Cankurt[62] measured with small particles of a cracking catalyst are shown in Fig. 12 for the bubbling, turbulent, and fast bed. The results are interpreted as a dependence of the slip velocity on the void fraction of bed. As the results suggest this relationship between the slip velocity and porosity is reasonably defined for the bubbling and turbulent bed. However, it is not the case of the fast fluidization where the slip velocity considerably increases with the increased rate of solids feeding.

As mentioned above, small particles tend to form relatively large aggregates or clusters that desintegrate and form again at appreciable frequencies. The slip velocities of such aggregates are often by an order of magnitude greater than the terminal fall velocity of the individual particles. All these facts contribute to efficient gas–solid contacting.

Fast fluidized or transport reactors[63–70] exhibite strong radial gradients, with the content of particles near the column walls higher than in the core of the reactor. Simple core/annulus (two-zone) models for circulating fluidized beds assume upflow of gas and entrained solids in a dilute central core and downflow of dense clusters in a relatively thin annular zone near the walls. There also exists some variation in the solids concentrations along the height of the column. It has been recognized that the overall geometric configuration of the column has also a profound effect on the gradients in both directions through the influence on the overall hydrodynamic behavior.

Circulating fluidized beds operated in the regime of fast fluidization have been employed for some gas–solid reactions including combustion of various fuels, gasification, calcination and dry scrubbing of gas.

Advantages of the regime of fast fluidization in respect to the bubbling, and turbulent beds include higher gas throughput, control of residence time of particles, reduced

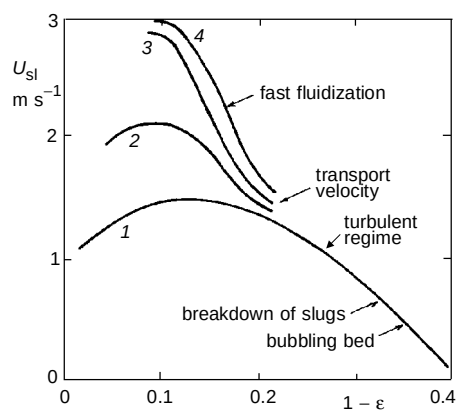

FIG. 12
Different regimes of the fluidized bed of catalyst particles[62]. Column diameter 0.15 m, $\bar{d}_p$ = 0.049 mm, ρ_s = 1 070 kg m^{-3}. The respective curves refer to the different rates of solids feeding: *1* 19.5 kg m^{-2} s^{-1}, *2* 97.6 kg m^{-2} s^{-1}, *3* 146 kg m^{-2} s^{-1}, *4* 195 kg m^{-2} s^{-1}

tendency of particles to agglomerate, and possibility of staged addition of gaseous reactants at different levels. Erosion appears to be a serious problem in some of the circulating fluidized beds.

The behavior of high velocity fluidized beds has been still little understood. There is not a reliable way of predicting the transitions from one hydrodynamic regime to another. As experience indicates, the entry, exit and wall configurations have an important influence on the flow and mixing patterns of both phases inside the columns.

Design of the units with high velocity fluidized beds cannot be made without practical experience. With small/light particles, Yerushalmi and Cankurt[62] ensured a stable regime and efficient contact at the superficial gas velocities around 3 – 4.6 m s^{-1} and high rates of solids recirculation.

All the operation modes of gas–solid systems are shown in the regime map that appears in Fig. 13. Basic characteristics and features of the respective modes of fluidization are summarized in Tables II and III. Predictive relationships have been reviewed for the onset of fluidization (U_{mf}) as well as for the terminal velocity of isolated particles (U_t) in refs[5,6].

5. CONCLUSIONS

The picture of bed of a particulate material fluidized with gas (fluid) widely varies in dependence on the physical properties of both phases as well as on the gas flow rate. The geometric factors have also an important influence on the flow pattern and gas–solid contacting within the vessel.

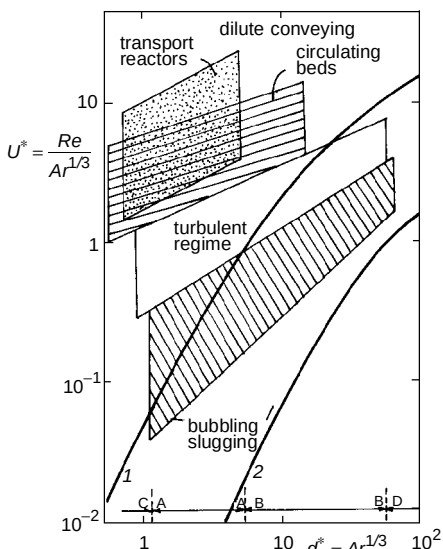

FIG. 13
Mapping of fluidization regimes adapted from Grace[67] and Reh[71]. Approximate boundaries between the different groups of Geldart's classification[11] are shown in the lower part of the diagram. *1* U_t, *2* U_{mf}

The state of the knowledge is quite developed for the bubbling bed of smaller/lighter particles (Geldart's Group A) operated at lower gas velocities. However it is not the case of large/heavy particles, particularly in the regimes of high velocity fluidization which is the least understood. More research effort is needed to explore the role of particle size distribution and to examine the influence of other factors as particle shape, particle density and physical properties of gas. For example, data on the hydrodynamic behavior of such systems at elevated temperature and pressure are practically lacking.

It should be stated that it is only the minimum fluidization velocity, U_{mf}, the minimum bubbling velocity, U_{mb}, and the terminal fluid velocity, U_t, which can be predicted for monosized, spherical particles with very good accuracy (i.e., better than 5 – 10%).

The predicting capabilities for U_{mf}, U_{mb}, and U_t are not that good for non-spherical particles which are generally used in practical situations.

Estimates of all the other transitions as well as the data given in Table III and Fig. 13 can be taken only as feasible approximations.

The fluidized beds operated in various modes require adequate different models which account for their observed nonhomogeneities. Flow or contacting pattern is of particular importance in cases of highly exothermic or endothermic reactions or where a high degree of conversion is needed. Attempts seem to be promising to extend some bubbling bed models to fast fluidization and other lean-phase contactors such as the circulating fluidized bed[72].

SYMBOLS

Ar	$= d_p^3 \boldsymbol{g} \rho_f (\rho_s - \rho_f)/\mu_f^2$, Archimedes number
C_1	parameter in Eq. (*8*)
C_2	parameter in Eq. (*8*)
d_b	diameter of bubble, m
d_{b0}	initial diameter of bubble, m
d_p	diameter of particles, usually mean sieve size, m
$\bar{d}_p$	mean particle diameter, m
d_p^*	dimensionless diameter of particle defined by Eqs (*3*) and (*5*)
D	diameter of column, m
F	cross-sectional area of the fluidized bed, m^2
Fr	$= U^2 \rho_f/(d_p \boldsymbol{g} (\rho_s - \rho_f)) = Re^2/Ar$, Froude number
$\boldsymbol{g}$	$= 9.807$ m s^{-2}, acceleration due to gravity
h	distance above the distributor, m
H	height of bed, m
H_L	critical height of bed for slugging, m
H_{mf}	height of bed at the minimum fluidization point, m
H_s	height of fixed bed, m
n	exponent in the Richardson–Zaki-type equation
Re	$= U d_p \rho_f/\mu_f$, Reynolds number
Re_c	$= U_c d_p \rho_f/\mu_f$, Reynolds number at the onset of decrease in mean amplitude of pressure fluctuations

Re_k	$= U_k\, d_p\, \rho_f/\mu_f$, Reynolds number at the point where the decrease in mean amplitude levels off
Re_{mb}	$= U_{mb}\, d_p\, \rho_f/\mu_f$, Reynolds number at the minimum bubbling point
Re_{mf}	$= U_{mf}\, d_p\, \rho_f/\mu_f$, Reynolds number at the minimum fluidization point
Re_t	$= U_t\, d_p\, \rho_f/\mu_f$, Reynolds number at the terminal free fall velocity
T	temperature, K
U	superficial velocity of fluid, m s^{-1}
U_b	velocity of bubbles, m s^{-1}
U_c	velocity of gas at which the mean amplitude of pressure fluctuations begins to decrease, m s^{-1}
U_{cf}	fluid velocity at complete fluidization of polydisperse system, m s^{-1}
U_e	$= U_{mf}/\varepsilon_{mf}$, interstitial velocity, m s^{-1}
U_k	velocity of gas at which the decrease in mean amplitude of pressure fluctuations levels off, m s^{-1}
U_{mb}	velocity at the point of minimum bubbling, m s^{-1}
U_{mf}	velocity at the point of minimum fluidization, m s^{-1}
U_{ms}	velocity at the point of minimum slugging, m s^{-1}
U_s	mean velocity of particles, m s^{-1}
U_{sl}	$= (U/\varepsilon) - U_s$, slip velocity, m s^{-1}
U_t	terminal free fall velocity of isolated particle in infinite medium, m s^{-1}
U_{tr}	transport velocity, m s^{-1}
U^*	dimensionless velocity defined by Eqs (*4*) and (*6*)
y	ratio of the actual visible bubble flow rate to the gas flow rate given by $(U - U_{mf})\, F$
δ	empirical parameter of Hilligardt and Werther[47]
γ	$= \boldsymbol{g}\,(\rho_s - \rho_f)$, specific weight of particles minus their specific buoyancy, kg m^{-2} s^{-2}
ε	bed voidage (void fraction or porosity of bed)
ε_b	fraction of bed volume occupied by bubbles at level h
$\bar{\varepsilon}_b$	overall fraction of bed volume occupied by bubbles
ε_{mb}	bed voidage at the point of minimum bubbling
ε_{mf}	bed voidage at the point of minimum fluidization
μ_f	fluid viscosity, kg m^{-1} s^{-1}
ρ_f	fluid density, kg m^{-3}
ρ_g	gas density, kg m^{-3}
ρ_s	particle density (bulk), kg m^{-3}
τ	time, s
ψ	sphericity of particle, shape factor

Financial support of the Grant Agency of the Academy of Sciences of the Czech Republic (Grant No. 472113) and of the Grant Agency of the Czech Republic (Grants No. 101/94/0112 and 203/94/0111) are gratefully acknowledged.

REFERENCES

1. Yates J. G.: *Fundamentals of Fluidized-Bed Chemical Processes*, p. 2. Butterworths, London 1983.
2. Kunii D., Levenspiel O.: *Fluidization Engineering*, p. 10, 2nd ed.. Butterworth–Heinemann, Boston 1991.

3. Hartman M., Svoboda K., Vesely V., Ziolkowski D.: Chem. Listy *81*, 1233 (1987).
4. Hartman M., Vesely V. in: *Encyclopedia of Fluid Mechanics, Suppl. 2* (N. P. Cheremisinoff, Ed.), p. 137. Gulf Publ. Co., Houston 1993.
5. Hartman M., Yates J. G.: Collect. Czech. Chem. Commun. *58*, 961 (1993).
6. Hartman M., Coughlin R. W.: Collect. Czech. Chem. Commun. *58*, 1213 (1993).
7. Geldart D.: *Gas Fluidization Technology*, p. 33, Wiley, Chichester 1986.
8. Wallis G. B.: *One-Dimensional Two-Phase Flow*, p. 21. McGraw–Hill, New York 1969.
9. Foscolo P. U., Gibilaro L. G., Di Felice R.: Appl. Sci. Res. *48*, 315 (1991).
10. Brandani S., Foscolo P. U.: Chem. Eng. Sci. *49*, 611 (1994).
11. Geldart D.: Powder Technol. *7*, 285 (1973).
12. Hartman M., Svoboda K., Vesely V.: Chem. Listy *79*, 247 (1985).
13. Geldart D., Harnby N., Wong A. C.: Powder Technol. *37*, 25 (1984).
14. Geldart D., Wong A. C.: Chem. Eng. Sci. *39*, 1481 (1984).
15. Svoboda K., Hartman M.: AIChE J. *27*, 866 (1981).
16. Svoboda K., Hartman M.: Ind. Eng. Chem., Process Des. Dev. *20*, 319 (1981).
17. Hartman M., Svoboda K.: Ind. Eng. Chem., Process Des. Dev. *26*, 649 (1986).
18. Pattipati R. R., Wen C. Y.: Ind. Eng. Chem., Process Des. Dev. *20*, 705 (1981).
19. Martin P. D.: Chem. Eng. Res. & Design *61*, 318 (1983).
20. Sciazko M., Bandrowski J.: Chem. Eng. Sci. *40*, 1861 (1985).
21. Molerus O.: Powder Technol. *33*, 81 (1982).
22. Rietema K.: Powder Technol. *37*, 5 (1984).
23. Pettyjohn E. S., Christiansen E. B.: Chem. Eng. Prog. *44* (2), 157 (1948).
24. Hartman M., Trnka O., Svoboda K.: Ind. Eng. Chem. Res. *33*, 1979 (1994).
25. Hartman M., Trnka O., Svoboda K., Vesely V.: Collect. Czech. Chem. Commun. *59*, 2583 (1994).
26. Grace J. R.: Can. J. Chem. Eng. *64*, 353 (1986).
27. Bandrowski J., Kolon P., Sciazko M.: Inzyn. Chem. *9*, 659 (1979).
28. Kmiec A.: Chem. Eng. J. *23*, 133 (1982).
29. Hartman M., Havlin V., Svoboda K., Kozan A. P.: Chem. Eng. Sci. *44*, 2770 (1989).
30. Hartman M., Trnka O., Havlin V.: Chem. Eng. Sci. *47*, 3162 (1992).
31. Fletcher J. V., Deo M. D., Hanson F. V.: Powder Technol. *69*, 147 (1992).
32. Dejong J. A. H., Nomden J. F.: Powder Technol. *9*, 91 (1974).
33. Piepers H. W., Cottaar E. J. E., Verkovijen A. H. M., Rietema K.: Powder Technol. *37*, 55 (1984).
34. Hoffmann A. C., Yates J. G.: Chem. Eng. Commun. *41*, 133 (1986).
35. Davies L., Richardson J. F.: Trans. Inst. Chem. Eng. *44*, 293 (1966).
36. Richardson J. F., Zaki W. N.: Trans. Inst. Chem. Eng. *32*, 35 (1954).
37. Garside J., Al-Dibouni M. R.: Ind. Eng. Chem., Process Des. Dev. *16*, 206 (1977).
38. Ziolkowski D., Michalski J., Hartman M., Svoboda K.: Inz. Chem. Proces. *4*, 603 (1989).
39. Hirata A., Bulos F. B.: J. Chem. Eng. Jpn. *23*, 599 (1990).
40. Ziolkowski D., Michalski J., Hartman M., Svoboda K.: Inz. Chem. Proces. *6*, 217 (1991).
41. Haider A., Levenspiel O.: Powder Technol. *58*, 63 (1989).
42. Godard K., Richardson J. F.: Inst. Chem. Eng. (London), Symp. On Fluodization 126 (1968).
43. Abrahamsen A. R., Geldart D.: Powder Technol. *26*, 35 (1980).
44. Broadhurst T. E., Becker H. A.: AIChE J. *21*, 238 (1975).
45. Hartman M., Vesely V., Trnka O., Svoboda K.: Collect. Czech. Chem. Commun. *52*, 1178 (1987).
46. Hartman M., Vesely V., Svoboda K.: Collect. Czech. Chem. Commun. *56*, 822 (1991).

47. Hilligardt K., Werther J.: Ger. Chem. Eng. *9*, 215 (1986).
48. Davidson J. F., Harrison D. in: *Fluidization* (J. F. Davidson and D. Harrison, Eds), p. 148. Academic Press, London 1971.
49. Mori S., Wen C. Y.: AIChE J. *21*, 109 (1975).
50. Rowe P. N.: Chem. Eng. Sci. *31*, 285 (1976).
51. Darton R. C., La Nauze R. D., Davidson J. F., Harrison D.: Trans. Inst. Chem. Eng. *55*, 274 (1977).
52. Tamarin A. I., Teplickii J. S.: Inzh.-Fiz. Zh. *32*, 469 (1977).
53. Chitester D. C., Kornosky R. M., Fan L.-S., Danko J. P.: Chem. Eng. Sci. *39*, 253 (1984); and references therein.
54. Catipovic N. M., Jovanovic G. N., Fitzgerald T. J.: AIChE J. *24*, 543 (1978).
55. Cranfield R. R., Geldart D.: Chem. Eng. Sci. *29*, 935 (1974).
56. Svoboda K., Cermak J., Hartman M., Drahos J., Selucky K.: AIChE J. *30*, 513 (1984).
57. Bayens J., Geldart D.: Chem. Eng. Sci. *29*, 225 (1974).
58. Lanneau K. P.: Trans. Inst. Chem. Eng. *38*, 125 (1960).
59. Kehoe P. W. K., Davidson J. F.: Inst. Chem. Eng. (London), Symp. Ser. *33*, 97 (1971).
60. Yang W. C.: AIChE J. *30*, 1025 (1984).
61. Brereton C. M. H., Grace J. R.: Trans. Inst. Chem. Eng. *70*, 246 (1992).
62. Yerushalmi J., Cankurt N. T.: Powder Technol. *24*, 187 (1979).
63. Bi H., Fan L.-S.: AIChE J. *38*, 297 (1992).
64. Staub F. W., Canada G. S. in: *Fluidization* (J. F. Davidson and D. L. Keairns, Eds), p. 339. Cambridge University Press, Cambridge 1978.
65. Sun G., Grace J. R.: AIChE J. *38*, 716 (1992).
66. Satija S., Fan L.-S.: AIChE J. *31*, 1554 (1985).
67. Grace J. R.: Chem. Eng. Sci. *45*, 1953 (1990).
68. Dry R. J.: Powder Technol. *49*, 37 (1986).
69. Dry R. J.: Powder Technol. *52*, 7 (1987).
70. Hannes J., Svoboda K.: Presented at *25th Meeting of the Int. Energy Agency on AFB Combustion, Riso, Denmark, 1992.*
71. Reh L.: Chem. Eng. Prog. *67*, 58 (1971).
72. Kunii D., Levenspiel O.: Ind. Eng. Chem. Res. *29*, 1226 (1990).